*Computational and Mathematical Methods in Medicine*,
Vol. 9, No. 1, March 2008, 47–67

Taylor & Francis
Taylor & Francis Group

# Modeling and simulation of a bacterial biofilm that is controlled by pH and protonated lactic acids

HASSAN KHASSEHKHAN and HERMANN J. EBERL*

Department of Mathematics and Statistics, University of Guelph, Guelph, ON, Canada N1G 2W1

*(Received 14 August 2006; revised 11 October 2007; in final form 25 October 2007)*

We present a mathematical model for growth and control of facultative anaerobic bacterial biofilms in nutrient rich environments. The growth of the microbial population is limited by protonated lactic acids and the local pH value, which in return are altered as the microbial population changes. The process is described by a non-linear parabolic system of three coupled equations for the dependent variables biomass density, acid concentration and pH. While the equations for the dissolved substrates are semi-linear, the equation for bacterial biomass shows two non-linear diffusion effects, a power law degeneracy as the dependent variable vanishes and a singularity in the diffusion coefficient as the dependent variable approaches its *a priori* known threshold. The interaction of both effects describes the spatial spreading of the biofilm. The interface between regions where the solution is positive and where it vanishes is the biofilm/bulk interface. We adapt a numerical method to explicitly track this interface in $x$–$t$ space, based on the weak formulation of the biofilm model in a moving frame. We present numerical simulations of the spatio-temporal biofilm model, applied to a probiotic biofilm control scenario. It is shown that in the biofilm neighbouring regions co-exist in which pathogenic bacterial biomass is produced or killed, respectively. Furthermore, it is illustrated how the augmentation of the bulk with probiotic bacteria leads to an accelerated decay of the pathogenic biofilm.

*Keywords*: Bacterial biofilm; Degenerate diffusion; Numerical simulation; Lactic acids; pH

*AMS Subject Classification*: 92C17; 35K65; 65C20; 65M50

## 1. Introduction

Bacteria, good or bad, tend to colonize surfaces that are immersed in aqueous environments. Planktonic cells attach to the surface (the so-called substratum) and become sessile. The bacteria produce extracellular polymers (EPS) that form a gel-like layer in which the cells themselves are embedded. Their number increases by cell division and vivid, highly organized microbial communities develop. Such biofilms form wherever nutrients are available to sustain microbial life, which makes them one of the most successful life forms on Earth [25].

*Corresponding author. Email: heberl@uoguelph.ca

*Computational and Mathematical Methods in Medicine*
ISSN 1748-670X print/ISSN 1748-6718 online 
http://www.tandf.co.uk/journals
DOI: 10.1080/17486700701797922

Biofilm occurrence reaches from beneficially engineered systems, mainly in environmental applications [47] such as wastewater treatment, soil remediation or bio-barriers for groundwater protection to unwanted ones. Most bacterial infections in the human body encountered by physicians are thought to be caused by such microbial communities, including many that are associated with biofouling on medical devices such as catheters, prosthetis and heart valves. The long list of biofilm related diseases includes cystic fibrosis pneumonia, prosthetic valve endocarditis, childhood ear infections, chronic prostatitis and dental cavities; see Refs. [8,13,14] for more extensive examples. Biofilms forming on production surfaces in food processing industry can cause food spoilage and pose hygienic risks [43,45] that again eventually can lead to disease. As an example, we give the hardy, harmful, food borne, biofilm forming pathogen *Listeria monocytogenes* that is found, *e.g.* in dairy products [36,44], and causes the often fatal infection listeriosis. Thus, prevention and eradication of biofilms is also of great food safety, hygienic and public health concern.

Life in biofilm communities offers protection against harmful environmental impacts that suspended cultures do not have. It was found that biofilm communities are much more difficult to eradicate with antimicrobial agents and antibiotics than their free swimming planctonic counterparts. Antibiotics kill the bacteria in the outer layers of the biofilm, i.e. close to the water/biofilm interface, but they fail to penetrate into the deeper layers of the EPS matrix. This leaves the cells close to the substratum largely unbothered and gives them time to develop resistance patterns against the particular antibiotics. Moreover, in many biofilms the cells in the inner layers are only scantily supplied with essential substrates, such as nutrients or oxygen (in the case of aerobic biofilms). As a consequence, they slow down their metabolism. In such a slow or even no-growth mode, the bacteria are also less susceptible to antibiotics and, hence, have increased chances of surviving such an attack. Once the environmental conditions become better, *e.g.* after the antibiotic wave passed and competing substrate consumers in the outer layers fell victim to the biocide, these dormant cells re-vitalize and re-populate the biofilm community. Moreover, in order to better facilitate the community's response to antibiotics exposure, certain bacteria develop quorum sensing communication strategies. The best studied example in this category is *Pseudomonas aeruginosa*, which plays a major role in cystic fibrosis pneumonia. A more detailed description of these biofilm defence mechanisms against antibiotics is given, *e.g.* in Refs. [8,41]. Furthermore, since the bacteria are immobilized in the sticky EPS network and adhere to the growth surface they are better protected against mechanical wash-out than free swimming bacteria. Hence, occurrence and growth of unwanted biofilm communities are difficult to control.

Mathematical models of biofilm processes traditionally focus on the growth of beneficial biofilms and the degradation of dissolved substrates [1,11,16,18,19,29,34,47] or on the disinfection of biofilms with antibiotics, antimicrobials or biocides [2,7,12,17,21,27,35,37–40,42]; Ref. [2] contains also a model for a novel quorum sensing based biofilm treatment strategy. In the present paper, we focus on a mathematical model for a different possible control mechanism of unwanted bacterial pathogens. We consider a facultative anaerobic bacterial population in a nutrient rich environment. Under these circumstances, neither oxygen nor nutrient availability is the controlling factor of biofilm formation. Instead, we investigate biofilm control by pH and protonated lactic acids, both of which can be detrimental to such bacterial populations. One possible realization of such a bio-control system is to augment the microbial ecology with harmless bacteria, the presence of which lowers the pH value until it reaches a value under which the pathogenic bacteria cannot easily thrive or even survive. An example is control of *L. monocytogenes* by *Lactococcus lactis*

populations, which are frequently developed as probiotics and added to dairy products as health promoting functional foods, e.g. [33]. Such a microbial system, under planktonic conditions, was studied experimentally and by mathematical modeling in Ref. [4], where competitive growth of both species in nutrient rich vegetable broth was considered. While nutrients are not limited in this system, it is the combined effect of pH and protonated acids that influences the growth activity. Moreover, the concentration of protonated acids is increased by the microbes, and higher concentrations of protonated acids, in return, imply lower pH. Thus, both quantities, pH and the protonated lactic acid concentration are the limiting substances for bacterial growth. Accordingly, the model that was proposed, calibrated and studied numerically in Ref. [4] is a nonlinear system of ordinary differential equations for the dependent variables biomass of pathogen and control agent, protonated acids and hydrogen ions.

In the present study, we investigate the potential of such a pH based control strategy for biofilm communities. This requires to consider the spatial organization of the biofilm and the diffusive transport in the EPS matrix. To this end, we adapt the ordinary differential equation model of Ref. [4] in the context of a previously introduced double degenerate parabolic model of biofilm formation [16]. The model of Ref. [4] appears in this density-dependent diffusion model in form of the reaction terms. The equations describing the limiting substrates become semi-linear diffusion–reaction equations. The spatial operator for biofilm spreading shows two non-standard diffusion effects: (i) a power law degeneracy, as in the case of the porous medium equation, for vanishing biomass densities and (ii) a singularity in the diffusion coefficient as the biofilm fully compresses. Both effects together lead to the development of sharp and steep interfaces in the model solution that mark the separation of the actual biofilm from its liquid environment. Such propagating interface problems in partial differential equations often are difficult to treat numerically. A promising new numerical approach for such interface propagation problems was suggested in Ref. [3], based on a weak formulation of the governing partial differential equation in a moving frame. This method was applied in Ref. [28] to a biofilm model with unlimited growth. We will adapt a modified version of this scheme for the biofilm control model.

The paper is organized as follows: In section 2, the mathematical model is formulated based on the non-linear diffusion model for spatio-temporal biofilm formation that was suggested in Ref. [16] and the reaction kinetics for pH-controlled bacterial populations that were established in Ref. [4]. In section 3, a fully adaptive numerical method is devised, based on a variable transformation that was adapted for the degenerated biofilm equation in Ref. [15], a weak moving frame formulation of the model that was developed in Ref. [3], and a time-scale argument, which goes back to Ref. [29] and is routinely used in most biofilm modeling studies. Simulation results are presented and discussed in section 4.

## 2. Model formulation

The biofilm model is formulated in terms of the active biomass density $N(t, x)$ in a spatial domain $\Omega$; here the independent variable $t \geq 0$ denotes time and the independent variable $x \in \Omega$ is the spatial location. The actual biofilm is the region in which the biomass is present, $\Omega_2(t) = \{x \in \Omega : N(t,x) > 0\}$, while the region $\Omega_1(t) = \{x \in \Omega : N(t,x) = 0\}$ is the liquid phase surrounding the biofilm. Both regions change as the biofilm grows. The biofilm structure $\Omega_2(t)$ can consist of several sub-regions that are not necessarily connected. We denote the biofilm/liquid interface by $\gamma$ and have $\gamma(t) = (\Omega_1(t) \cap \bar{\Omega}_2(t))\backslash\partial\Omega$.

Following Ref. [16], biofilm formation is described by the nonlinear evolution equation

$$\partial_t N = \nabla\cdot(D(N)\nabla N) + g(C,P)N, \tag{1}$$

where the density-dependent diffusion coefficient for biofilm spreading has the form

$$D(N) = d\frac{N^b}{(N_{\max}-N)^a}, \quad a,b \geq 1, \quad d > 0. \tag{2}$$

Thus, the diffusion operator of (1) shows two non-linear effects: (i) a power law degeneracy as in the porous medium equation such that $D(0) = 0$ and (ii) a power law singularity as $N$ approaches to the maximum possible cell density, $N \longrightarrow N_{\max}$ (fast diffusion). The first effect (i) guarantees that the biofilm does not spread notably if the biomass density is small, $N \ll N_{\max}$, and it is also responsible for the formation of a sharp interface between biofilm and surrounding liquid, *i.e.* initial data with compact support lead to solutions with compact support. The second effect (ii) ensures that the maximum biomass density is not exceeded. Both effects together are required to describe biofilm formation (squeezing property). Biofilm diffusion models of this type have been studied in a small series of papers, both analytically and numerically in Refs. [15–23,28].

The net growth rate $g(C, P)$ in (1) depends on the local concentration of protonated acids, $C$, and hydrogen ions, $P$. The latter measures the pH value such that increasing $P$ means decreasing pH and vice versa, more specific we have

$$\mathrm{pH} = -\log_{10} P,$$

with $P$ measured in mole. The growth function is positive (growth phase) if both values $C$, $P$ are small and negative (decay phase) if at least one of them is large. Between both extrema a plateau phase is observed. For our study, we use the continuous and piecewise linear growth function that was suggested and experimentally verified in Ref. [4] for suspended cultures of *L. monocytogenes* and *L. lactis* in vegetable broth

$$g(C,P) = \mu\cdot\min\left\{1 - \frac{C}{H_1(C)}, 1 - \frac{P}{H_2(P)}\right\}, \tag{3}$$

where the auxiliary functions $H_1(C)$ and $H_2(P)$ are defined by

$$H_1(C) = k_1 H(k_1 - C) + C\cdot H(C - k_1)\cdot H(k_2 - C) + k_2 H(C - k_2),$$

and

$$H_2(P) = k_3 H(k_3 - P) + P\cdot H(P - k_3)\cdot H(k_4 - P) + k_4 H(P - k_4).$$

Here, the function $H$ is defined by

$$H(x) = \begin{cases} 1, & \text{if } x > 0 \\ \frac{1}{2} & \text{if } x = 0 \\ 0, & \text{if } x < 0 \end{cases}$$

Parameters $\mu$, $k_{1,2,3,4}$ are positive constants with $k_1 < k_2$ and $k_3 < k_4$. The growth function $g(C, P)$ of (3) is plotted in figure 1 for a typical set of parameters that were estimated from

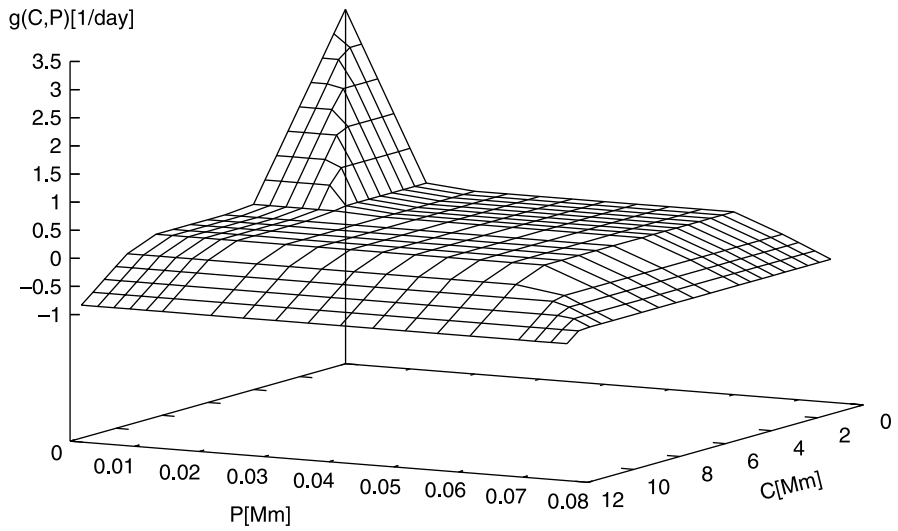


Figure 1. Piecewise linear, continuous net growth rate $g(C, P)$ using parameters as suggested by Ref. [4]. The population grows, $g > 0$, for small values of $C$ and $P$ and decays, $g < 0$, if either concentration $C$ or $P$ becomes large; the region in between marks the neutral, stationary phase.

laboratory experiments in Ref. [4]. We note that the function $g(C, P)$ in (3) is Lipschitz continuous in the positive cone $C > 0$, $P > 0$ with respect to both of its arguments. The Lipschitz constant can be estimated from the model parameters $k_1$ through $k_4$.

Protonated lactic acids $C$ are produced locally in the presence of bacteria until the concentration reaches a saturation value $C_{\max}$ with $C_{\max} > k_2$. Assuming first order kinetics as proposed in Ref. [4] for suspended cultures and taking diffusive transport of protonated acids into account one obtains

$$\partial_t C = \nabla \cdot (D_c(N)\nabla C) + \kappa N\left(1 - \frac{C}{C_{\max}}\right), \tag{4}$$

where $\kappa$ is a positive rate constant. Protonated acids lower the pH value, i.e. lead to an increase of $P$ until a saturation value $P_{\max}$ is reached with $P_{\max} > k_4$. Following again, the first order reaction kinetics identified in Ref. [4] for suspended cultures and considering diffusive transport, one obtains similar to (4) the diffusion–reaction equation for $P$,

$$\partial_t P = \nabla(D_p(N)\nabla P) + \rho C\left(1 - \frac{P}{P_{\max}}\right), \tag{5}$$

where again $\rho$ is a positive rate constant.

Equations (1), (4) and (5) with (2) and (3) represent a nonlinear system of diffusion–reaction equations for the dependent variables biomass density $N$, concentration of protonated acids $C$ and concentration of hydrogen ions $P$. It is completed by a set of initial data and appropriate boundary conditions. These will be specified later on.

Note that the diffusion coefficients in (4) and (5) depend on the local biomass density $N$. More specifically, we have

$$D_c(N) = \begin{cases} d_c, & N = 0 \\ \tau_c d_c, & N > 0 \end{cases}, \quad \text{and} \quad D_p(N) = \begin{cases} d_p, & N = 0 \\ \tau_p d_p, & N > 0 \end{cases}, \tag{6}$$

where the positive constant $d_c$ is the diffusion coefficient of protonated acids in the liquid phase. In the biofilm matrix, diffusion of dissolved substrates is typically somewhat slower than in the bulk liquid environment, depending on the size of the diffusing molecules [6]. We denote the ratio of the diffusion coefficients in biofilm and water by $\tau_c$ and have $0 < \tau_c \leq 1$; the quantities $d_p$ and $\tau_p$ are defined accordingly for the diffusion parameters of $P$. For the diffusion coefficient of $P$, we make similar assumptions. In particular with definition (6), transport of $C$ and $P$ is due to regular Fickian diffusion in both domains, biofilm and liquid environment. Across the biofilm/liquid interface $\gamma$, the concentrations $C$ and $P$ are continuous but have a crack, *i.e.* are discontinuous in the normal derivative if $0 < \tau_c < 1$ or $0 < \tau_p < 1$, respectively. Thus, the solutions of (4) and (5) are to be understood in the weak sense. Continuity of the diffusive flux mandates

$$[\partial_n(D_c(N)C)]_\gamma = 0 \quad \text{and} \quad [\partial_n(D_p(N)P)]_\gamma = 0, \tag{7}$$

where $[\cdot]_\gamma$ denotes a jump discontinuity at $\gamma$, and $\partial_n$ denotes the derivative in normal direction at the interface $\gamma$. Interface condition (7) can be derived formally with the divergence theorem after integrating (4) and (5) over $\Omega$ and separating the domain along $\gamma$. Continuity of the concentration across the interface can be expressed in the same notation by

$$[C]_\gamma = 0 \quad \text{and} \quad [P]_\gamma = 0. \tag{8}$$

The numerical method that will be devised in the next section explicitly locates the position of the biofilm/water interface, which will allow to explicitly enforce the interface conditions (7) and (8) and to treat (4) and (5) piecewise as semi-linear equations.

In the following, we will use a re-formulation of (1), in terms of the volume fraction $u$ occupied by biomass, $u = N/N_{\max}$. Then, the biofilm equation becomes

$$u_t = \nabla \cdot \left( \varepsilon \frac{u^b}{(1-u)^a} \nabla u \right) + g(C,P)u, \quad a, b > 1,\ \varepsilon > 0, \tag{9}$$

with

$$\varepsilon = dN_{\max}^{b-a}.$$

*Remark*. The specific, piecewise linear growth function (3) was introduced in Ref. [4] to capture the three main stages of bacterial growth curves, as observed in laboratory experiments: growth phase, stationary phase and decay phase, as defined, *e.g.* in Ref. [30]. In the modeling literature, however, smooth functions are generally preferred, for reasons of regularity of model solutions. A typical smooth inhibition model for $C$ and $P$ controlled

bacterial growth is described by the growth rate (all parameters positive)

$$\tilde{g}(C,P) = \mu\left(\frac{\kappa_C}{\kappa_C + C}\right)^{m_C}\left(\frac{\kappa_P}{\kappa_P + P}\right)^{m_P} - \delta,$$

which behaves qualitatively similar to (3), albeit without the extended almost stationary phase that is observed in experiments. The numerical method described below can be applied to such a model as well without modifications. Nevertheless, we will keep the piecewise linear reaction rate (3) introduced in Ref. [4], for the remainder of this paper.

*Remark*. Existence and long-term behavior of solutions of the initial-boundary value problem of a biofilm model that shows the same degenerate-diffusion behaviour as (9), but with a Monod reaction term that describes production of new biomass (and accordingly changed evolution equations for the controlling nutrient) was studied analytically in Ref. [22]. One of the key results in that paper was the existence of a global attractor, the structure of which was explored in Ref. [20]. Additional analytical results can be found in Ref. [15] for biofilms with unlimited growth, where in particular a variable transformation was introduced that will be utilized in our numerical method in the next section. A generalization of the existence proof to biofilms formed by more than one particulate substance was developed in Ref. [21].

## 3. Numerical method

We will derive a weak moving frame form of equation (9), based on which a moving mesh finite element algorithm will be constructed that explicitly tracks the movement of the biofilm/liquid interface. This idea follows the concept outlined in Ref. [3] and was applied to a similar model of a biofilm, albeit with uncontrolled growth, in Ref. [28]. We modify this approach here by performing a change in the dependent variables, which transforms the degenerated diffusion operator into the Laplace operator and shifts all non-linear diffusion effects of (9) into the time derivative. This idea is carried over from Ref. [15] where it was used for the discretization of the biofilm model on a fixed, non-adaptive grid. The substrate equations (4) and (5) must be solved in the liquid phase $\Omega_1(t)$ as well. Since these are semi-linear diffusion–reaction equations with no further peculiarities, any standard solver for this type of equations can be applied. For the time-treatment of the transport-reaction equations, we invoke a standard argument of biofilm modeling [1,29,34,47]. The characteristic time scales of the diffusion and reaction processes governing the concentration fields of dissolved substrates are much smaller than those of biofilm formation and spreading. Therefore, a quasi steady state assumption is made for (4) and (5). Thus, this system is converted into two elliptic problems, one for each of $C$ and $P$, at every time-step of the biofilm growth model. In fact, due to the special form of the reaction terms, the system for $P$ and $C$ at every time-step can be solved as two consecutive scalar linear equations.

### *3.1. Model formulation in the moving frame and computational realization*

The normalized biomass equation (9) can be re-written in the form

$$\partial_t u - \varepsilon\Delta\Phi(u) = g(C,P)u, \tag{10}$$

with

$$\Phi(u) = \int_0^u \frac{s^b}{(1-s)^a}\,\mathrm{d}s = \frac{u^{b+1}}{b+1}\mathcal{F}(a, b+1; 2+b; u), \tag{11}$$

where

$$\mathcal{F}(a, b+1; 2+b; u) = \sum_{k=0}^{\infty} \frac{u^k}{k!}\frac{\Gamma(k+a)\Gamma(k+1+b)\Gamma(2+b)}{\Gamma(a)\Gamma(b+1)\Gamma(k+2+b)},$$

is the hypergeometric function. In all applications of the density-dependent diffusion-operator to biofilm modeling, the exponents are chosen such that $a, b \in \mathbb{N}$. Then, one obtains

$$\Phi(u) = \frac{u^{b+1}}{b+1}\mathcal{F}(a, b+1; b+2; u) = \sum_{k=0}^{\infty} \binom{k+a-1}{k} \frac{u^{k+b+1}}{k+b+1}.$$

For example, the specific choice $a = 2 + b$, $b \in \mathbb{N}$ leads to the simple expression

$$\Phi(u) = \frac{1}{a-1}\frac{u^{a-1}}{(1-u)^{a-1}}. \tag{12}$$

For certain other choices of $a, b \in \mathbb{N}$, the integrals in (11) can be found in the literature, e.g. in Ref. [5]. In any case, for given $a$, $b \geq 1$, the solution of the integral in (11) can be represented as an analytical real function. Following Ref. [15], we introduce the new dependent variable $v$, defined by

$$v =: \Phi(u). \tag{13}$$

Since $\Phi$:[0,1) $\rightarrow$ [0,$\infty$) is a strictly increasing function, it is also invertible. We introduce the inverse

$$\beta(v) \coloneqq \Phi^{-1}(v) = u. \tag{14}$$

It is easy to show that $\beta : [0, +\infty) \rightarrow [0, 1)$ is an increasing function as well; *e.g.* in the case $b = a - 2 \in \mathbb{N}$, cf. (12), we have $u = \beta(v) = (((a-1)v)/(1+(a-1)v))^{1/(a-1)})$. Re-writing (10) in terms of the new dependent variable $v$ we obtain finally

$$\beta(v)_t - \varepsilon\Delta v = g(C, P)\beta(v). \tag{15}$$

In order to derive a moving frame formulation of (15), we denote by $\xi$ the points in the initial biofilm domain $\Omega_2(0) = \{\xi \in \Omega : \beta(v(\xi, 0)) > 0\}$ and by $\hat{x}$ an invertible map that describes the trajectories of these points in the moving frame such that

$$x = \hat{x}(\xi, t), \tag{16}$$

defines the biofilm region, $\Omega_2(t) = \{x \in \Omega : \beta(v(x, t)) > 0\}$. For the purpose of explicitly tracking the interface between biofilm and liquid phase, we require that under $\hat{x}$ the boundary of $\Omega_2(0)$ is mapped to the boundary of $\Omega_2(t)$. More specifically, we require that the interface $\gamma(0)$ is mapped into $\gamma(t)$ and that the points in $\partial\Omega_2(0) \cap \partial\Omega$ remain stationary. The map $\hat{x}$ that satisfies these conditions will be specified below. With the same change of independent

variables, $v$ can be presented in moving form as well, *i.e.*

$$v(x,t) = v(\hat{x}(\xi,t),t) \coloneqq \hat{v}(\xi,t), \tag{17}$$

from which

$$\frac{\partial \hat{v}}{\partial t} = \frac{\partial \hat{x}}{\partial t}\cdot\nabla v + \frac{\partial v}{\partial t} = \frac{\mathrm{d}v}{\mathrm{d}t}. \tag{18}$$

We define also

$$\beta(v(x,t)) = \beta(\hat{v}(\xi,t)) \coloneqq \hat{\beta}(v), \tag{19}$$

and introduce the notation

$$\dot{\beta}(v) = \frac{\mathrm{d}\hat{\beta}(v)}{\mathrm{d}t}, \qquad \dot{x} = \frac{\mathrm{d}\hat{x}}{\mathrm{d}t},$$

Thus,

$$\dot{\beta}(v) = \beta'(\hat{v})\frac{\mathrm{d}\hat{v}}{\mathrm{d}t} = \beta'(v)\left(\nabla v\cdot\frac{\mathrm{d}x}{\mathrm{d}t} + \frac{\partial v}{\partial t}\right) = \beta'(v)\nabla v\cdot\dot{x} + \frac{\mathrm{d}\beta}{\mathrm{d}t}, \tag{20}$$

where with (14), the derivative $\beta'(v)$ with respect to $v$ reads

$$\beta'(v) = \frac{1}{\Phi'(u)} = \frac{(1-\beta(v))^a}{\beta(v)^b}.$$

We obtain the moving frame formulation of (15)

$$\dot{\beta}(v) - \frac{(1-\beta(v))^a}{\beta(v)^b}\nabla v\cdot\dot{x} - \varepsilon\Delta v = g(C,P)\,\beta(v). \tag{21}$$

For the convenience of notation, we abbreviate (15) by

$$\beta(v)_t = Lv, \tag{22}$$

where $L$ is the semi-linear diffusion–reaction operator, *i.e.*

$$Lv \coloneqq \varepsilon\Delta v + g(C,P)\beta(v).$$

In order to calculate the interface location, we shall derive the weak formulation of (15) in the moving frame as given by (16) and (21). Taking into account that $\beta(v) \equiv 0$ in $\Omega_1(t) = \Omega\backslash\Omega_2(t)$ and applying the Divergence Theorem in $\Omega_2(t)$, we obtain the integral version of the governing equation (22)

$$\frac{\mathrm{d}}{\mathrm{d}t}\int_{\Omega_2(t)}\beta(v)\mathrm{d}x = \int_{\Omega_2(t)}\frac{\partial\beta(v)}{\partial t}\mathrm{d}x + \oint_{\partial\Omega_2(t)}\beta(v)\dot{x}\cdot n\,\mathrm{d}s = \int_{\Omega_2(t)}\left(\frac{\partial\beta(v)}{\partial t} + \nabla\cdot(\beta(v)\dot{x})\right)\mathrm{d}x, \tag{23}$$

where $n$ is the outward pointing unit normal vector to $\partial\Omega_2(t)$. Let us assume that $\omega$ belongs to the space of test functions with compact support, satisfying the linear advection equation

$$\frac{\partial \omega}{\partial t} + \dot{x} \cdot (\nabla \omega) = 0. \tag{24}$$

Then, we obtain finally from (21), the weak form of (22) in the moving frame

$$\frac{\mathrm{d}}{\mathrm{d}t}\int_{\Omega_2(t)} \omega\beta(v)\mathrm{d}x - \int_{\Omega_2(t)} \omega\nabla\cdot(\beta(v)\dot{x})\mathrm{d}x = \int_{\Omega_2(t)} \omega\, Lv\,\mathrm{d}x. \tag{25}$$

It remains to determine the mapping (16). Following Ref. [3], this will be based on the principle of conservation of mass. To this end, we calculate the total (normalized) biomass in the system $\theta(t)$ as

$$\theta(t) = \int_{\Omega_2(t)} \beta(v)\mathrm{d}x, \tag{26}$$

and obtain for the test function $\omega$

$$\int_{\Omega_2(t)} \omega\beta(v)\mathrm{d}x = \delta\theta(t), \tag{27}$$

which defines $\delta$. From (25) and (27), we derive

$$\delta\dot{\theta}(t) - \int_{\Omega_2(t)} \omega\nabla\cdot(\beta(v)\dot{x})\mathrm{d}x = \int_{\Omega_2(t)} \omega\, Lv\,\mathrm{d}x, \tag{28}$$

and after integration by parts,

$$\delta\dot{\theta}(t) - \int_{\partial\Omega_2(t)} \omega\beta(v)\dot{x}\cdot n\,\mathrm{d}s + \int_{\Omega_2(t)} \beta(v)\dot{x}\cdot\nabla\omega\,\mathrm{d}x = \int_{\Omega_2(t)} \omega\, Lv\,\mathrm{d}x. \tag{29}$$

In order to calculate the velocity of the moving points uniquely, the concept of vorticity is introduced, which is equal to the curl of the velocity, following Ref. [3]. Therefore, for given $\theta$ and $u$ from (29) and for a known point vorticity, a point velocity potential function $\phi$ is defined such that $\dot{x} = \nabla\phi$. We obtain from (29)

$$\delta\dot{\theta}(t) - \int_{\partial\Omega_2(t)} \omega\beta(v)\nabla\phi\cdot n\,\mathrm{d}s + \int_{\Omega_2(t)} \beta(v)\nabla\phi\cdot\nabla\omega\,\mathrm{d}x = \int_{\Omega_2(t)} \omega\, Lv\,\mathrm{d}x. \tag{30}$$

In order to compute $\dot{x}$ and $\dot{\theta}$, we obtain with

$$\int_{\Omega_2(t)} \omega\cdot\dot{x}\,\mathrm{d}x = \int_{\Omega_2(t)} \omega\cdot\nabla\phi\,\mathrm{d}x, \tag{31}$$

so that

$$\dot{\theta}(t) = \int_{\Omega_2(t)} (Lv + \nabla \cdot (\beta(v)\dot{x}))\mathrm{d}x. \tag{32}$$

After integration and incorporating the boundary condition, $\dot{\theta}$ simplifies to

$$\dot{\theta}(t) = \int_{\Omega_2(t)} g(C,P)\beta(v)\mathrm{d}x. \tag{33}$$

Integrating by parts and using the compact support properties of the test functions $\omega$, we derive from (25)

$$\delta\dot{\theta}(t) = -\varepsilon \int_{\Omega_2(t)} \nabla v \cdot \nabla \omega \, \mathrm{d}x + \int_{\Omega_2(t)} g(C,P)\beta(v)\omega \, \mathrm{d}x + \int_{\Omega_2(t)} \omega \nabla \cdot (\beta(v)\nabla\phi)\mathrm{d}x, \tag{34}$$

where we used the velocity potential function $\dot{x} = \nabla\phi$ and (27). From this equation, we can calculate $\phi$ and, hence, the grid velocity $\dot{x}$ from equation (31). Note that by this procedure points that lie initially on the biofilm/liquid interface $\gamma(0)$ will be mapped on to points on the biofilm/liquid interface $\gamma(t)$ for all $t > 0$.

To approximate the continuous weak formulation by a discrete representation, we introduce a finite set of basis functions $\omega_i$, $i = 1, \ldots, M$. Conservation of mass mandates that these are chosen such that $\sum_{i=1}^{M} \omega_i = 1$ and thus

$$\sum_{i=1}^{M} \int_{\Omega_2(t)} \omega_i \beta(v)\mathrm{d}x = \sum_{i=1}^{M} \delta_i \theta(t) = \theta(t), \tag{35}$$

with

$$\sum_{i=1}^{M} \delta_i = 1. \tag{36}$$

For the computational realization of the interface tracking algorithm, we discretize the equations of the previous section and solve them for a finite number of moving points $X_i(t)$ in the domain. This is essentially an adaptation of the moving grid technique in Ref. [3] for our model equation (9) in the transformed form (15). Later on, in the numerical examples, we shall use piecewise linear basis functions.

We introduce a disjoint finite element segmentation of the initial domain $\Omega_2(0)$. Let us assume that the initial grid points

$$X(0) = (X_1(0), X_2(0), X_3(0), \ldots, X_M(0))^{\mathrm{T}},$$

$X_i(0) \in \Omega$ are given, not necessarily equidistant over the whole domain $\Omega_2(0)$ at time $t = 0$. We denote by $\{W_i(x,t)\}_{i=1,\ldots,M}$ the set of basis functions. The basis functions change over time, *i.e.* they are adapted to the moving grid points $X_j(t)$. They satisfy $W_i(X_j(t),t) = \delta_{ij}$ for all $t$, satisfy the advection equation (24) and the first of (36). The local weights $c_i$ = const associated with the basis functions can be computed *a priori* from the initial data and (35) and (36).

We approximate the solution $u = \beta(v)$ of (9) in the grid points $X_j(t)$ by

$$\beta(v(X_j(t), t)) \approx \beta(V_j(t)) = \sum_{i=1}^{M} \beta(V_i(t)) W_i(X_j(t), t), \tag{37}$$

where the approximation of the transformed dependent variable $V_i(t) = V(X_i, t)$ and the approximation of the original dependent variable $U_i(t)$ of $u(X_i(t), t)$ relate like

$$V_i(t) = \int_0^{U_i(t)} \frac{s^b}{(1-s)^a} \mathrm{d}s. \tag{38}$$

The discrete velocity potential of the moving grid reads

$$\phi_j(t) \coloneqq \phi(X_j(t), t) = \sum_{i=1}^{M} \phi_i(t) W_i(X_j(t), t). \tag{39}$$

With this discretization, we derive from (30), (31) and (33) a system of ordinary differential equations for the movement of the grid points and the rate of change of mass

$$\frac{\mathrm{d}}{\mathrm{d}t} \begin{pmatrix} X \\ \theta \end{pmatrix} = F \begin{pmatrix} X \\ \theta \end{pmatrix}. \tag{40}$$

We have a dynamical system which monitors the location of the moving mesh points and the total biomass in the system. The solution $u = \beta(v)$ is obtained by integrating (15) over the moving domain spanned by (40). The system of ordinary differential equations (40) can be solved numerically using an appropriate Ordinary Differential Equation (ODE) solver. In our simulations in the next section, we use a time-adaptive Runge–Kutta–Fehlberg method of order 4(5) [24]. The right hand side of (40) is evaluated in several steps. To this end, discrete versions of the equations discussed above must be computed.

### *3.2. Computation of C and P*

When formulating the weak moving frame version of model (1) and its numerical approximation, we always assumed $C(t, x)$ and $P(t, x)$ as known functions. We comment here briefly on the computation of these two quantities. First, we note that for the calculation of the concentration fields in the biofilm region $\Omega_2(t)$, also the concentration fields in the liquid region $\Omega_1(t)$ must be computed, due to the coupling across the interface (7) and (8). Note that in particular the equation (4) for $C$ simplifies greatly in the liquid region where $N \equiv 0$. The governing equations (4) and (5) are semi-linear diffusion–reaction equations, the spatial discretizations of which do not pose special difficulties. Since the location of the biofilm/liquid interface is explicitly known from section 3.1, the interface conditions (7) and (8) can be enforced. For the time-treatment of the transport-reaction equations, we invoke a standard argument of biofilm modeling [1,29,34,47]. The diffusion and reaction processes governing the concentration fields of dissolved substrates are much faster than those governing biofilm formation and spreading. Therefore, a quasi steady state assumption is made for (4) and (5). First, a time-step $t_{j-1} \rightarrow t_j$ of the growth model is calculated based on the previous values $C(t_{j-1}, \cdot)$, $P(t_{j-1}, \cdot)$, $N(t_{j-1}, \cdot)$, resulting in $N(t_j, \cdot)$ at the new time level.

Then, the concentration fields $C(t_j, \cdot)$ and $P(t_j, \cdot)$ relax to the equilibrium

$$0 = \nabla(D_{\mathrm{c}}(N)\nabla C) + \kappa N\left(1 - \frac{C}{C_{\max}}\right), \tag{41}$$

$$0 = \nabla(D_{\mathrm{p}}(N)\nabla P) + \rho C\left(1 - \frac{P}{P_{\max}}\right), \tag{42}$$

for known biomass density $N(t_j, \cdot)$. Since $N(t, \cdot)$ is known from section 3.1, equation (41) is a linear equation for $C(t_j, \cdot)$. After obtaining $C(t_j, \cdot)$, the equation (42) reduces to a linear elliptic equation for concentration field $P(t_j, \cdot)$.

In recent years, much emphasis in biofilm modeling was placed on the complicated morphological structure, in which many biofilms develop [1,11,16,31,34], such as mushroom-shaped or pillar-shaped architectures that are characteristic for many biofilm systems. It was shown previously that the density-dependent diffusion mechanism is able to predict such structures [16,18,19,47]. However, the bacterium *L. monocytogenes* that is the model species for this study is known to form rather thin, flat biofilms, *e.g.* [19,26]. Therefore, in the numerical model illustrations in the next section, we will restrict ourselves to spatially one-dimensional simulations where the biofilm grows perpendicular to the substratum as a homogeneous layer. The equation (41) reduces then to the ordinary boundary value problem

$$\begin{cases} \tau_{\mathrm{c}} d_{\mathrm{c}} C'' = -\kappa\beta(v)\left(1 - \frac{C}{C_{\max}}\right) & x \in [0, \gamma(t_j)] \\ C'' = 0 & x \in [\gamma(t_j), L]\,, \\ C(t_j, L) = C_{\infty,j}, C'(t_j, 0) = 0, [C]_\gamma = 0, [D_C(N)C']_\gamma = 0 \end{cases} \tag{43}$$

where $C_{\infty,j}$ is the Dirichlet value for $C$ at time level $t_j$. Due to absence of biomass in the liquid region, the concentration field can be solved there analytically. One obtains for $\gamma(t_j) < x < L$

$$C(t_j, x) = \frac{C_{\infty,j} - C_{\gamma(t_j)}}{L - \gamma(t_j)}x - \frac{\gamma C_{\infty,j} - C_{\gamma(t_j)}}{L - \gamma(t_j)}, \tag{44}$$

which can be used to construct a Robin boundary condition for $C$ in $\Omega_2$. Thus, the boundary condition depends on the interface position which is a function of time. Equation (43) for the biofilm region $0 < x < \gamma(t_j)$ becomes

$$C'' = -\frac{\kappa\beta(v)}{\tau_{\mathrm{c}} d_{\mathrm{c}}}\left(1 - \frac{C}{C_{\max}}\right), \tag{45}$$

with

$$C'(0) = 0, \quad (L - \gamma(t_j))C'(\gamma(t_j)) + \gamma(t_j)C(\gamma(t_j)) = (\gamma(t_j) - L)C_{\infty,j}. \tag{46}$$

In order to avoid interpolation, equation (45) is solved on the mesh that is constructed for the discretization of $u$ as outlined above in section 3.1. Since this mesh changes adaptively, appropriate non-equidistant finite difference formula are required. Using the standard second order compact stencil discretization of the second derivative, *e.g.* [32], leads to a linear

system described by a tridiagonal $M$-matrix. Thus, its inverse exists and is positive, which ensures the existence of a positive numerical solution of (45) with (46).

Similarly, (42) leads to the piecewise defined linear ordinary boundary value problem

$$P'' = -\frac{\rho}{\tau_{\mathrm{p}} d_{\mathrm{p}}} C\left(1 - \frac{P}{P_{\max}}\right), \quad 0 < x < \gamma(t_j), \tag{47}$$

and

$$P'' = -\frac{\rho}{d_{\mathrm{p}}} C\left(1 - \frac{P}{p_{\max}}\right) \quad \gamma(t_j) < x < L, \tag{48}$$

with the coupling conditions

$$[D_P(N)P']_\gamma = 0, \quad [P]_\gamma = 0, \tag{49}$$

and boundary conditions

$$P'(0) = 0, \quad P(L) = P_{\infty,j}. \tag{50}$$

The concentration $C$ in this problem is determined as the solution of (43) and (44). Again, standard second order finite differences are used to solve (47)–(50).

## 4. Numerical simulations

### *4.1. General system description and model behavior*

For our simulations, we consider the following general description of a biofilm reactor that is frequently made in one dimensional biofilm modeling (figure 2). The physical system is subdivided into three distinct phases: (i) the actual biofilm, attached to an impermeable surface, in which the bacterial biomass is concentrated, corresponding to $\Omega_2$ in our notation above, (ii) a concentration boundary layer in the surrounding liquid phase, in which $P$ and $C$ undergo gradients (this is $\Omega_1$; see also Ref. [47] for a more detailed description of the

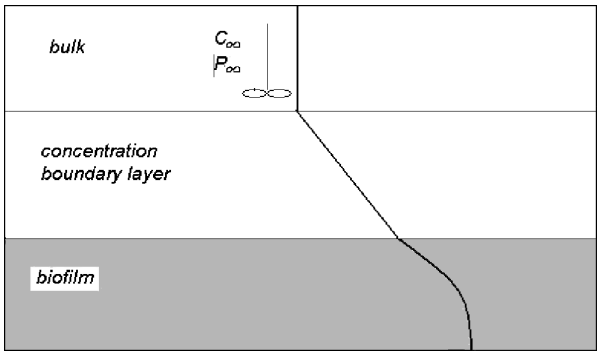


Figure 2. The biofilm system is described by three phases: the actual biofilm $\Omega_2$, the concentration boundary layer $\Omega_1$, and the bulk liquid, which is described in the model by the boundary conditions. The plotted curve schematically indicates the profile of concentrations $C$ and $P$ in the system.

concentration boundary layer concept) and (iii) the bulk liquid, which is assumed to be completely mixed. In our model, the bulk liquid is described by the boundary conditions for $C$ and $P$. We make the usual assumption that the reactor is sufficiently large such that the concentrations in the bulk liquid are not affected by the bio-chemical reactions in the biofilm. The biofilm processes are controlled by controlling the concentration in the bulk liquid.

Since pathogenic biofilms like *L. monocytogenes* can often be found in non- or extremely slow flowing systems [26] we can assume the concentration boundary layer to be thick compared to the biofilm, $\gamma(0) \ll L$.

The boundary conditions posed on the bacterial biomass are a homogeneous Neumann condition at the impermeable substratum and a homogeneous Dirichlet conditions at the (moving) biofilm/liquid interface, *i.e.*

$$\partial_x u|_{x=0} = 0, \qquad u(t, \gamma(t)) = 0, \quad t > 0. \tag{51}$$

**4.1.1 Implications of the maximum principle**. The boundary conditions for $C$ and $P$ were specified above in section 3.2. The maximum principle for two-point boundary value problems [46] implies that in every time step, i.e. for a given biomass distribution $u(t_j, x) > 0$ for $x < \gamma(t_j)$ and $u(t_j, x) = 0$ in $x > \gamma(t)$, both concentration fields $C$ and $P$ attain their minimum on the Dirichlet boundary $x = L$, are monotonous functions for $0 < x < L$, and attain their maximum at the Neumann boundary $x = 0$, *i.e.* at the substratum. Physically, this is due to the interaction of Fickian diffusion and production in the biofilm. The observation of increasing $P$ with increasing penetration depth into the biofilm is equivalent to decreasing pH with increasing penetration depth. This is consistent with typical pH profile measurements in biofilms, *e.g.* [9,48] and with simulation studies in Ref. [10] for the neutral pH range. Note that the model in Ref. [10] is a more detailed description of pH than the one discussed here, but does not account for the effect of pH on the biofilm.

From the comparison principle, it follows that the concentrations $C$ and $P$ in the domain are the higher, the higher the boundary values $C_{\infty,j}$ and $P_{\infty,j}$ are. In particular, it is implied that in every time step the solutions of (41) and (42) are unique and positive, moreover, they are bounded like $0 \le C \le C_{\max}$ and $0 \le P \le P_{\max}$ iff $0 \le C_\infty \le C_{\max}$ and $0 \le P_\infty \le P_{\max}$.

With this observation, it is clear that biofilm growth is only possible if the boundary concentrations of $C$ and $P$ are sufficiently small. For values $C_\infty$ and $P_\infty$ in the neutral region $g(C_\infty,P_\infty) = 0$ or in the region $g(C_\infty,P_\infty) < 0$ of decay, cf. figure 1, no growth will be observed but probably local degradation of the viable biomass of the biofilm. If $C_\infty$ and $P_\infty$ are small enough to allow for biomass production, we expect the microbial production activity to be stronger close to the biofilm liquid/interface and to decrease inside the biofilm toward the substratum. Eventually, due to microbial activity the concentrations $C$ and $P$ in the biofilm will be high enough to have microbial decay or a neutral zone in the inner layers while there still might be new biomass produced at the outer layers.

Note that this behaviour is quite different from what is observed in biofilm control with antibiotics. As pointed out in our introduction, antibiotics are typically successful in killing the cells in the outer layers but often fail to penetrate the entire biofilm, leaving the cells in the inner layers unharmed; this was also observed and verified in simulation studies of a antibiotic disinfection model based on the same density-dependent diffusion description of biofilm formation and growth [17,21].

**4.1.2 Simulations**. Our expectations of model behaviour deduced from qualitative analytical arguments are confirmed by the simulation results in figure 3, based on the reaction parameters determined experimentally in Ref. [4] for a culture of *L. monocytogenes* in vegetable broth, *cf* also table 1; the simulations were carried out for small constant values of $C_\infty$ and $P_\infty$ (clearly in the range $g(C_\infty, P_\infty) > 0$) and constant inital data for $u$ in the biofilm. Initially, the biofilm grows slightly. Due to diffusion and reaction of the controlling substrates $C$ and $P$ the biomass distribution in the biofilm is non-uniform, *i.e.* one observes biomass gradients from the substratum to the interface. Thus, higher microbial activity is observed close to the biofilm/liquid interface $\gamma(t)$, where new biomass is produced and the biofilm compresses. In the inner layers, no new biomass is produced. This behaviour is controlled by $C$ and $P$. Both increase from the boundary to the substratum. $C$ undergoes a boost in the biofilm due to the production terms that are active in the presence of biomass. This boost in $C$ and the subsequent growth of $P$ lead to concentration values high enough to have $g(C, P) \leq 0$ in the biofilm, and thus a stop in production of new bacteria.

### *4.2. Application to a biocontrol system*

In a simple numerical study, we consider the following bio-control system: at time $t = 0$ a small suspended population of a harmless bacterium is added to the bulk liquid that promotes the production of $C_\infty$ and $P_\infty$. We denote the density of this population by $N_2$. Such a bacterium that has been used for the control of the pathogen *L. monocytogenes* is the gram positive facultative anaerobic *L. lactis*, e.g. [4,36], that can be developed as a probiotic and added as a functional food to dairy products. The fate of the population of *L. lactis* and its

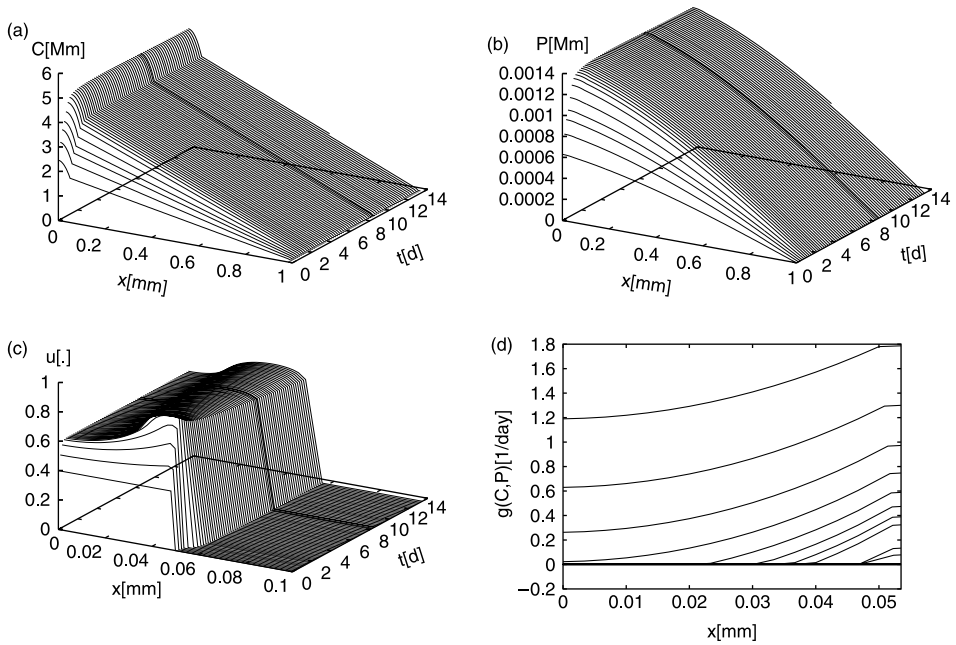


Figure 3. Simulation of (4), (5) and (9): shown are $C(t, x)$ (top left), $P(t, x)$ (top right), $u(t, x)$ (bottom left). Also included is the local growth rate inside the biofilm, $g(C, P)$ (bottom right), for selected time steps. The uppermost line corresponds to $t_0$; for increasing $t$, $g(C, P)$ decreases due to an increase of $C$ and $P$.

Table 1. Parameters used in the simulations in section 4. Reaction parameters are taken from Ref. [4], transport parameters have been adapted from Ref. [16].

| Parameters | Units | Values |
|---|---|---|
| $\mu$ (lab) | $d^{-1}$ | 2.5176 |
| $\mu$ (*Listeria*) | $d^{-1}$ | 3.5304 |
| $\kappa$ (*Listeria*) | $Mm\,CFU^{-1}\,d^{-1}$ | $7.08 \times 10^{-9}$ |
| $\kappa_2$ (lab) | $Mm\,CFU^{-1}\,d^{-1}$ | $4.08 \times 10^{-9}$ |
| $k_1$ (lab) | Mm | 5.2 |
| $k_1$ (*Listeria*) | Mm | 4.05 |
| $k_2$ (lab) | Mm | 8.907 |
| $k_2$ (*Listeria*) | Mm | 8.907 |
| $C_{max}$ (*Listeria*) | Mm | 11.65 |
| $C_{max,2}$ (lab) | Mm | 11.5 |
| $k_3$ (lab) | Mm | 0.03935 |
| $k_3$ (*Listeria*) | Mm | 0.01282 |
| $k_4$ (lab) | Mm | 0.07129 |
| $k_4$ (*Listeria*) | Mm | 0.07063 |
| $P_{max}$ (lab) | Mm | 0.07413 |
| $P_{max_2}$ (*Listeria*) | Mm | 0.07556 |
| $\rho$ | $Mm\,CFU^{-1}\,d^{-1}$ | $2.4 \times 10^{-4.472}$ |
| $\rho_2$ | $Mm\,CFU^{-1}\,d^{-1}$ | $2.4 \times 10^{-4.172}$ |
| $d_c$ | $m^2\,d^{-1}$ | $4.97 \times 10^{-5}$ |
| $d_p$ | $m^2\,d^{-1}$ | $8.16 \times 10^{-5}$ |
| $\tau_c$ | – | 0.898 |
| $\tau_p$ | – | 0.9302 |
| $\varepsilon$ | – | $10^{-9}$ |
| $a$, $b$ | – | 4 |

effect on the bulk concentrations of protonated acid and proton ion is described by the following ordinary differential equation, which has the same structure as a corresponding suspended culture model for *L. monocytogenes*, albeit with different model parameters

$$\frac{dN_2}{dt} = g_2(C_\infty, P_\infty)N_2, \tag{52}$$

$$\frac{dC_\infty}{dt} = \kappa_2 N_2 \left(1 - \frac{C_\infty}{C_{max,2}}\right), \tag{53}$$

$$\frac{dP_\infty}{dt} = \rho_2 C_\infty \left(1 - \frac{P_\infty}{P_{max,2}}\right), \tag{54}$$

where the growth function $g_2(C, P)$ of *L. lactis* is defined similarly as the growth function $g(C, P)$ of *L. monocytogenes* and all parameters are positive. In fact, (52) is the competition model [4] restricted to the *L. lactis* population only. The dynamic behaviour of this model is easily confirmed with standard arguments of qualitative ODE theory. The positive cone $(N_2, C, P) \geq 0$ is positively invariant as can be shown with the usual tangent criterion that can be found, *e.g.* in Ref. [46]. Thus, we have in particular $N_2 \geq 0$. With the same argument, it can be shown that $C_\infty \leq C_{max,2}$ and $P_\infty \leq P_{max,2}$, if $0 \leq C_\infty(0) \leq C_{max}$ and $0 \leq P_\infty(0) \leq P_{max}$. Due to monotonicity of the reaction terms in (53) and (54), we obtain that $C_\infty(t)$ and $P_\infty(t)$ are monotonously increasing functions such that $C_\infty \to C_{max,2}$ and $P_\infty \to P_{max,2}$ as $t \to \infty$.

The parameter estimation carried out in Ref. [4] showed that $C_{\max,2}$ and $P_{\max,2}$ are in the range of decay of $N_2$, i.e. $g_2(C_{\max,2}, P_{\max,2}) < 0$. This implies that $N_2 \to 0$ as $t \to \infty$.

We use the bulk concentration values $C_\infty(t)$ and $P_\infty(t)$ according to (52)–(54) as Dirichlet boundary values in our numerical simulation of the *L. monocytogenes* biofilm model (1), (4) and (5), recall also figure 2. The effect of this dynamic boundary condition on the concentration fields of $C$ and $P$ and on the biomass density $u$ in the biofilm system is observed in figures 4, compared to figures 3. It is obvious that both concentrations are raised in the concentration boundary layer as well as in the biofilm. Accordingly, the development of the biofilm is hampered and its decay starts earlier.

Several simulations of this type were carried out with a varying initial population size of $N_2$ in the bulk liquid. The corresponding solution surfaces $u(t, x)$ of the biofilm model are superimposed in figure 5 (left panel). It is observed that an increase in the density of the control population *L. lactis* in the bulk liquid implies a lower biomass density of *L. monocytogenes* in the biofilm and leads to its quicker decay. The total biomass of *L. monocytogenes* in the biofilm as a function of time and in dependence of the inital density of the control agent is plotted in the right panel of figure 5.

## 5. Conclusion

We formulated a mathematical model that is able to describe the effect of variations in pH and protonated lactic acids on a bacterial biofilm and used it in an idealized modeling study to investigate a bio-control mechanism that is based on adding beneficial bacterial cultures to

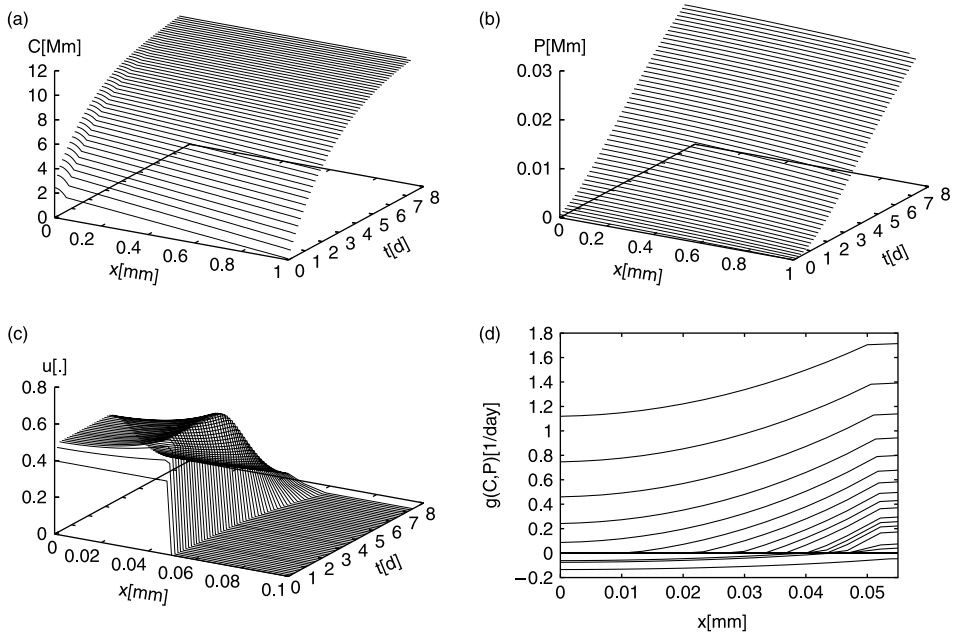


Figure 4. Simulation of (4), (5) and (9): shown are $C(t, x)$ (top left), $P(t, x)$ (top right), $u(t, x)$ (bottom left). Also included is the local growth rate inside the biofilm, $g(C, P)$ (bottom right), for selected time steps. The uppermost line corresponds to $t_0$; for increasing $t$, $g(C, P)$ decreases due to an increase of $C$ and $P$. The reaction parameters are the same as in figure 3 but boundary conditions have been changed to (52)–(54).

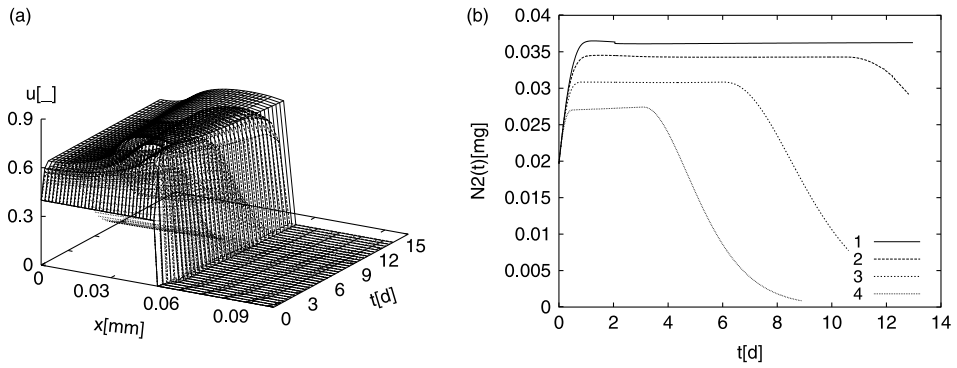


Figure 5. Effect of initial density of the control agent in the bulk liquid on the biofilm: shown are $u(t, x)$ (left) and the total amount of biomass $\int u(t, x)\mathrm{d}x$ (right). Lines 1–4 represent adding 0, 2, 4, 8 times 10E7 CFU of control agent in simulations.

a system that is infested by a harmful pathogenic biofilm. To this end, we combined an ODE model of the control system for suspended cultures with a degenerate parabolic spatio-temporal model of biofilm formation and adapted a numerical solver that is suitable for interface propagation problems in parabolic evolution equations. Quantitative numerical simulations and qualitative analytical and physical considerations lead to the conclusion that under this control mechanism the bacteria in the inner layers, close to the substratum, are affected first. In many instances, they will already be diminished while simultaneously the growth conditions are still favourable for the bacteria in the outer layers of the biofilm. This situation is quite different from traditional biofilm disinfection with antibiotics and biocides, where the bacteria in the inner layers are protected by the outer layer and the antibiotics fail to fully penetrate the biofilm. It seems, therefore, to be worthwhile to study the potential of a combined antibiotics/probiotics treatment strategy for biofilms, both experimentally and theoretically.

Based on this first modeling study, a less simplified model and an extended numerical experiment can be devised that allows to study the effect of probiotic cultures on pathogenic biofilms in a less idealized environment. In particular, it will be straightforward, albeit numerically more expensive, to include further controlling substrates such as nutrients and oxygen. While the simulations in this paper were carried out in a spatially one-dimensional set-up, the model has been developed for and is applicable to the general three-dimensional case as well.

## Acknowledgements

This study was supported in parts by Canada's Network Centers of Excellence program through the Advanced Foods and Material Network (AFMNET). HJE acknowledges also the support received from NSERC (Discovery Grant) and the Canada Research Chairs Program.

## References

[1] Alpkvist, E., 2005, Modelling and simulation of heterogeneous biofilm growth using a continuum approach. Licentiate thesis, Malmo University.

[2] Anguige, K., King, J.R. and Ward, J.P., 2005, Modelling antibiotic- and quorum sensing treatment of a spatially-structured *Pseudomonas aeruginosa* population, *Journal of Mathematical Biology*, **51**, 557–594.
[3] Baines, M.J., Hubbard, M.E. and Jimack, P.K., 2005, A moving mesh finite element algorithm for the adaptive solution of time dependent PDEs with moving boundaries, *Applied Numerical Mathematics*, **54**, 450–469.
[4] Breidt, F. and Flemming, H.P., 1998, Modeling of the competitive growth of *Listeria monocytogenes* and *Lactococcus lactis* in vegetable broth, *Applied and Environmental Microbiology*, **64**(9), 3159–3165.
[5] Bronstein, I.N. and Semendjajew, K.A., 1991, *Taschenbuch der Mathematik*, 25th ed. (Leipzig: Teubner).
[6] Bryers, J.D. and Drummond, F., 1998, Local macromolecule diffusion coefficients in structurally non-uniform bacterial biofilms using fluorescence recovery after photobleaching (FRAP), *Biotechnology and Bioengineering*, **60**(4), 462–473.
[7] Cogan, N.G., Cortez, R. and Fauci, L., 2005, Modeling physiological resistance in bacterial biofilms, *Bulletin of Mathematical Biology*, **67**(4), 831–853.
[8] Costerton, J.W., Stewart, P.S. and Greenberg, E.P., 1999, Bacterial biofilms: a common cause of persistent infections, *Science*, **284**(5418), 1318–1322.
[9] de Beer, D., Huisman, J.W., vanden Heuvel, J.C. and Ottengraf, S.P.P., 1992, The effect of pH profiles in methanogenic aggregates on the kinetics of acetate conversion, *Water Research*, **26**(10), 1329–1336.
[10] Dibdin, G.H., 1992, A finite-difference computer model of solute diffusion in bacterial films with simultaneous metabolism and chemical reaction, *CABIOS*, **8**(5), 489–500.
[11] Dockery, J. and Klapper, I., 2002, Finger formation in biofilm layers, *SIAM Journal of Applied Mathematics*, **62**, 853–869.
[12] Dodds, M.G., Grobe, K.J. and Stewart, P.S., 2000, Modeling biofilm antimicrobial resistance, *Biotechnology and Bioengineering*, **68**(4), 464–456.
[13] Donlan, R.M., 2001, Biofilms and device associated infections, *Emerging Infectious Diseases*, **7**(2), 277–281.
[14] Donlan, R.M., 2002, Biofilms: microbial life on surfaces, *Emerging Infectious Diseases*, **8**(9), 881–890.
[15] Duvnjak, A. and Eberl, H.J., 2006, Time-discretisation of a degenerate reaction–diffusion equation arising in biofilm modeling, *El. Trans. Num. Analysis*, **23**, 15–38.
[16] Eberl, H.J., Parker, D.F. and van Loosdrecht, M.C.M., 2001, A new deterministic spatio-temporal continuum model for biofilm development, *Journal of Theoretical Medicine*, **3**, 161–175.
[17] Eberl, H.J. and Efendiev, M.A., 2003, A transient density dependent diffusion–reaction model for the limitation of antibiotic penetration in biofilms, *El. Journal of Differential Equation CS*, **10**, 123–142.
[18] Eberl, H.J., 2004, A deterministic continuum model for the formation of EPS in heterogeneous biofilm architectures, Proc. Biofilms, Las Vegas.
[19] Eberl, H.J., Schraft, H., *et al.*, 2007, A diffusion–reaction model of a mixed culture biofilm arising in food safety studies. In: A. Deutsch (Ed.) *Mathematical Modeling of Biological System*, Vol. II (Birkhäuser).
[20] Efendiev, M.A. and Demaret, L., On the structure of attractors for a class of degenrate reaction–diffusion systems, to appear.
[21] Efendiev, M.A., Demaret, L., Lasser, R. and Eberl, H.J., Analysis and simulation of a meso-scale model of diffusive resistance of bacterial biofilms to penetration of antibiotics, submitted.
[22] Efendiev, M.A., Eberl, H.J. and Zelik, S.V., 2002, Existence and longtime behavior of solutions of a nonlinear reaction–diffusion system arising in the modeling of biofilms, *RIMS Kokyuroko*, **1258**, 49–71.
[23] Efendiev, M.A. and Müller, J., 2007, Classification of running fronts for fast diffusion, in preparation, submitted.
[24] Epperson, J.F., 2002, *An Introduction to Numerical Methods and Analysis* (New York: Wiley & Sons).
[25] Flemming, H.C., 2000, Biofilme—das Leben am Rande der Wasserphase, *Nachr. Chemie*, **48**, 442–447.
[26] Hassan, A.N., Birt, D.M. and Frank, J.F., 2004, Behavior of *Listeria monocytogenes* in a Pseudomonas putida biofilm on a condensate-forming surface, *Journal of Food Protection*, **67**(2), 322–327.
[27] Hunt, S.M., Hamilton, M.A. and Stewart, P.S., 2005, A 3D model of antimicrobial action on biofilms, *Water Science and Technology*, **52**(7), 143–148.
[28] Khassehkhan, H. and Eberl, H.J., 2006, Interface tracking for a non-linear, degenerated diffusion–reaction equation describing formation of bacterial biofilms, *DCDIS A*, **SA13**, 131–144.
[29] Kissel, J.C., McCarty, P.L. and Street, R.L., 1984, Numerical simulation of mixed-culture biofilm, *ASCE Journal of Environmental Engineering*, **110**(2), 393–411.
[30] Lee, Y.K., 2003, Bioprocess technology. In: Y.K. Lee (Ed.) *Microbial Biotechnology. Principles and Applications* (Singapore: World Scientific).
[31] Van Loosdrecht, M.C.M., Picioreanu, C. and Heijnen, J.J., 1997, A more unifying hypothesis for the structure of microbial biofilms, *FEMS Microbial Ecology*, **24**, 181–183.
[32] Morton, K.W. and Mayers, D.F., 1994, *Numerical Solution of Partial Differential Equations* (Cambridge: Cambridge University Press).
[33] O'Toole, D.K. and Lee, Y.K., 2003, Fermented foods. In: Y.K. Lee (Ed.) *Microbial Biotechnology. Principles and Applications* (Singapore: World Scientific).
[34] Picioreanu, C., 1999, Multi-dimensional modeling of biofilm structure. PhD thesis, TU Delft.
[35] Roberts, M.E. and Stewart, P.S., 2004, Modeling antibiotic tolerance in biofilms by accounting for nutrient limitation, *Antimicrobial Agents and Chemotherapy*, **48**(1), 48–52.

[36] Stecchini, M.L., Aquili, V. and Sarais, I., 1995, Behavior of *Listeria monocytogenes* in Mozarella cheese in the presence of *Lactococcus lactis*, *International Journal of Food Microbiology*, **25**(3), 301–310.
[37] Stewart, P.S., 1994, Biofilm accumulation model that predicts antibiotic resistance of *Pseudomonas aeruginosa* biofilms, *Antimicrobial Agents and Chemotherapy*, **38**(5), 1052–1058.
[38] Stewart, P.S. and Raquepas, J.B., 1995, Implications of reaction–diffusion theory for disinfection of microbial biofilms by reactive antimicrobial agents, *Chemical Engineering and Science*, **50**(19), 3099–3104.
[39] Stewart, P.S., 1996, Theoretical aspects of antibiotics diffusion into microbial biofilms, *Antimicrobial Agents and Chemotherapy*, **40**(11), 2517–2522.
[40] Stewart, P.S., Hamilton, M.A., Goldstein, B.R. and Schneider, B.T., 1996, Modelling biocide action against biofilms, *Biotechnology and Bioengineering*, **49**, 445–455.
[41] Stewart, P.S., *et al.*, 2003, BioLine Multicellular nature of biofilm protection from antimicrobial agents. In: A. McBain (Ed.) *Biofilm Communities: Order from Chaos*.
[42] Szomolay, B., Klapper, I., Dockery, J. and Stewart, P.S., 2005, Adaptive responses to antimicrobial agents in biofilms, *Environmental Microbiology*, **7**(8), 1186–1191.
[43] Trachoo, N., 2003, Biofilms and the food industry, *Songlanakarin Journal of Science and Technology*, **25**(6), 807–815.
[44] US Dept. of Health and Human Services, Centers for Disease Control and Prevention. The world wide web, url http://www.cdc.gov/ncidod/dbmd/diseaseinfo/listeriosis_g.htm, Date: October 2005.
[45] Verran, J., 2002, Biofouling in food processing: biofilm or biotransfer potential?, *Trans. IChemE.*, **80**(C), 292–298.
[46] Walter, W., 2000, *Gewöhnliche Differentialgleichungen*, 7th ed. (Berlin: Springer).
[47] Wanner, O., Eberl, H., Morgenroth, E., Noguera, D., Picioreanu, C., Rittmann, B. and van Loosdrecht, M.C.M., 2006, *Mathematical Modeling of Biofilms* (London: IWA Publishing).
[48] Zhang, T.C. and Bishop, P.L., 1996, Evaluation of substrate an pH effects in a nitrifying biofilm, *Water Environmental Research*, **68**(7), 1107–1115.